Going skin deep: a direct comparison of penetration potential of lipid-based nanovesicles on the isolated perfused human skin flap model

Selenia Ternullo[a], Louis de Weerd[b], Ann Mari Holsæter[a], Gøril Eide Flaten[a], Nataša Škalko-Basnet[a,*]

[a]Drug Transport and Delivery Research Group, Department of Pharmacy, University of Tromsø The Arctic University of Norway, Universitetsveien 57, 9037 Tromsø, Norway; Email: selenia.ternullo@uit.no (S.T.); ann-mari.holsater@uit.no (A-M.H.); goril.flaten@uit.no (G.E.F.)

[b]Department of Plastic and Reconstructive Surgery, University Hospital of North Norway, Sykehusvegen 38, 9019 Tromsø and Department of Clinical Medicine, University of Tromsø The Arctic University of Norway, Universitetsveien 57, 9037 Tromsø, Norway; Email: Louis.De.Weerd@unn.no (L.D.W.)

*Corresponding author: Nataša Škalko-Basnet, Drug Transport and Delivery Research Group, Department of Pharmacy, University of Tromsø The Arctic University of Norway, Universitetsveien 57, 9037 Tromsø, Norway; Tel: +47-776-46640; Fax: +47-776-46151; Email: natasa.skalko-basnet@uit.no

Abstract

Phospholipid-based nanocarriers are attractive drug carriers for improved local skin therapy. In the present study, the recently developed isolated perfused human skin flap (IPHSF) model was used to directly compare the skin penetration enhancing potential of the three commonly used nanocarriers, namely conventional liposomes (CLs), deformable liposomes (DLs) and solid lipid nanoparticles (SLNs). Two fluorescent markers, calcein (hydrophilic) or rhodamine (lipophilic), were incorporated individually in the three nanosystems. The nanocarrier size ranged between 200 and 300 nm; the surface charge and entrapment efficiency for both markers were dependent on the lipid composition and the employed surfactant. Both carrier-associated markers could not penetrate the full thickness human skin, confirming their suitability for dermal drug delivery. CLs exhibited higher retention of both markers on the skin surface compared to DLs and SLNs, indicating a depo formation. DLs and SLNs enabled the deeper penetration of the two markers into the skin layers. *In vitro* and *ex vivo* skin penetration studies performed on the cellophane membrane and full thickness pig/human skin, respectively, confirmed the findings. In conclusion, efficient dermal drug delivery can be achieved by the optimization of a lipid nanocarrier on the suitable skin-mimicking model to assure system's accumulation in the targeted skin layer.

polydispersity index; SC, *stratum corneum*; SDCh, sodium deoxycholate; SLNs, solid lipid nanoparticles.

1. Introduction

According to the Global Burden of Disease Study 2010, the skin diseases are the fourth leading cause of disease burden at global level. The skin-related illnesses are cause of the disability affecting between 30 and 70% of individuals [1]. Despite progress achieved in the local skin therapy, the treatment of skin diseases remains challenging [2]. Topical drug delivery for localized skin therapy bears some advantages compared to the traditional administration routes, such as the avoidance of systemic administration, the lower dose of drug required to reach the desired level at the targeted site and the reduction of systemic side effects [3]. In addition, an increase in the antimicrobial resistance among the drugs used to treat skin infections systemically, is emphasising the need for an efficient localized antimicrobial skin therapy [4]. However, the penetration of drugs into the deeper skin layers, especially through the *stratum corneum* (SC), remains an important challenge in the development of effective topical formulations destined to exert localized effect in the skin [5]. For example, in the inflammatory skin diseases (e.g. dermatitis, psoriasis) and fungal skin infections, leucocytes invade the skin leading to an increase in the proliferation and differentiation of keratinocytes and consequent increase in the skin thickness and further enhancement of the skin barrier properties exerted mainly by the SC [6]. The formulations that fail to achieve the optimal therapeutic drug levels within the deeper skin layers, or to assure the depot at the skin surface, are considered suboptimal. Among the emerging approaches employed to improve the dermal delivery of drugs, nanodermatology represents one of the most promising [7,8]. Nanocarriers have shown to improve the solubility of highly hydrophobic drugs, increase drug chemical and physical stability, deliver higher concentration of drugs to the targeted site and provide sustained and controlled release of the associated drugs [9]. Phospholipid-based nanosystems are of a particular interest and have been widely investigated for improving the topical skin therapy. Their phospholipid nature contributes to

low toxicity and high compatibility with physiological skin lipids, especially in the SC [10]. These lipid-based nanocarriers have shown to enhance the penetration through the skin by overcoming the intact skin barrier and allowing dermal delivery of associated drugs [11]. One of the first proposed vesicular nanosystems were the conventional liposomes (CLs). Their structure permits the incorporation of lipophilic, hydrophilic and amphiphilic compounds [12]. The similarities between CLs and skin lipids allow their accumulation on the SC surface and fusion with skin lipids. This induces changes in the SC intercellular lipids, thus increasing the skin permeability and drug penetration [10]. However, most of the literature proves that CLs remain mainly confined to the SC thus building a reservoir to release slowly ~~release~~ the associated drug. To improve drug penetration deeper into the skin layers, deformable liposomes (DLs) were proposed by Cevc and Blume [13]. These liposomes are composed of lipids and an edge activator, which provides elasticity and deformability to the liposomes. Consequently, DLs could potentially squeeze through the SC thus increasing the transport of the drug deeper into the skin layers [14].

Alternative to liposomes are particulate lipid-based nanosystems, such as solid lipid nanoparticles (SLNs). SNLs are composed of one or more solid lipids dispersed in an aqueous medium with an addition, if necessary, of a surfactant as a stabiliser [15]. These nanocarriers lack the bilayer structure of the liposomes, thus being more stable in both hydrophilic and lipophilic environment [16]. SLNs allow controlled release of the drug and penetration enhancement exerted by their occlusive properties [17]. Furthermore, they exhibit good skin tolerability, and are considered to be safe and biocompatible [18].

The lipid composition of the lipid-based nanocarriers is strongly influencing their physicochemical characteristics, such as particle size, surface charge, bilayer elasticity and thermodynamic phase. By optimizing the lipid composition, it is possible to

influence/optimize vesicle deposition onto/within the skin and modulate the depth to which the drug will be delivered [19].

For the first time, we directly compared the skin penetration enhancement of three different lipid-based nanocarriers on the isolated human skin flap (IPHSF) model, a recently developed human skin perfusion model [20]. To follow the drug penetration from different lipid-based nanocarriers, two fluorescent markers with different lipophilicities, calcein and rhodamine, were employed and their penetration from the CLs, DLs and SLNs followed. The IPHSF model offers the advantage of working with the skin in the presence of dermal circulation, thus mimicking the *in vivo* human conditions to a higher extent. The confocal laser scanner microscopy (CLSM) technique was used to follow the penetration profiles. Moreover, a comparison of the marker penetration on IPHSF model with some of the established skin penetration models such as cellophane membrane and full thickness pig/human full thickness skin in the Franz diffusion cells system was performed.

2. Materials and methods

2.1. Materials

Lipoid S 100 (phosphatidylcholine from soybean, >94% pure; PC) was a gift from Lipoid GmbH (Ludwigshafen, Germany). Calcein, rhodamine B, methanol CHROMASOLV®, magnesium sulfate heptahydrate, potassium chloride, sodium bicarbonate, sodium chloride, trichloroacetic acid (≥99.0%), Fiske-Subbarow reducer reagent, ammonium molybdate, phosphorus standard solution, sodium deoxycholate (SDCh) and Triton™ X-100 were purchased from Sigma-Aldrich Chemie (Steinheim, Germany). Potassium dihydrogen phosphate, glucose, hydrogen peroxide (30%) and calcium chloride were obtained from Merck KGaA (Darmstadt, Germany). Propylene glycol (PG) was purchased from NMD – Norwegian Medical Depot AS (Oslo, Norway), Albunorm® (human serum albumin, 200

mg/mL) from Octapharma AG (Lachen, Switzerland) and sucrose from VWR International bvba/sprl (Leuven, Belgium). Sulfuric acid was purchased from May and Baker LTD (Dagenham, UK). Cellophane membrane was obtained from Max Bringmann KG (Wendelstein, Germany) and pig ears from Nortura AS (Bardufoss, Norway).

2.2. Preparation of liposomes

CLs and DLs with calcein or rhodamine were prepared by the film hydration method [21]. PC (300 mg) for CLs or PC/SDCh (total 300 mg; 85/15 % as weight ratio) for DLs were dissolved in approximately 20 mL of methanol in a round bottomed flask. When applicable, rhodamine (47.9 mg) was dissolved together with the lipid in organic solvent resulting in 10 mM rhodamine solution. The organic solvent was completely removed under a vacuum (50 mbar) using a rotary vacuum evaporator (Büchi Rotavapor R-124 with Büchi Vacuum Pump V-700, Büchi Labortechnik AG, Flawil, Switzerland) for 1 h at 45 °C. The resulting lipid film was then rehydrated in 10 mL of modified Krebs-Henseleit buffer (KHb) (pH 7.40; 280 mOsm; 110 mM NaCl, 3.8 mM KCl, 1.4 mM KH_2PO_4, 1.2 mM $MgSO_4$, 31 mM $NaHCO_3$, 2.5 mM $CaCl_2$, 11 mM glucose and 10 mM sucrose) by hand shaking at room temperature (23-24 °C) for 20 min. For calcein-containing liposomes, calcein (62.2 mg) was dissolved in the KHb to form 10 mM calcein solution used to rehydrate the film. All liposomal suspensions were stored overnight in the fridge (+4 °C) prior to the characterisation.

2.3. Preparation of solid lipid nanoparticles

SLNs with calcein or rhodamine were prepared by the solvent injection method [22] with some modifications. PC (1.20 g) was dissolved in methanol. The obtained lipid solution (120 mg/mL; 2 mL) was then rapidly injected via an injection needle (Sterican® 0.30 x 12 mm,

Braun Melsungen AG, Melsungen, Malaysia) into KHb solution (6 mL) under the stirring (300 rpm). For SLNs containing calcein, the marker was dissolved in the KHb solution used to prepare nanoparticles, whereas for SLNs containing rhodamine, the lipophilic marker was dissolved in the lipid solution. Both markers were applied in the same concentrations as used for CLs and DLs preparation. The suspension was stirred for 2 h at room temperature (23-24 ºC) and kept overnight in the fridge (+4 ºC) prior to the characterisation.

2.4. Size reduction

The original size of CLs, DLs and SLNs containing either calcein or rhodamine was reduced by the hand extrusion through the polycarbonate membrane (Nuclepore® Track-Etched Membranes, Whatman House, Maidstone, UK). The pore size of the membranes and the number of extrusion cycles were adjusted for each formulation to obtain vesicles within the size range of 200-300 nm. CLs, DLs and SLNs containing calcein were extruded stepwise through the 0.8, 0.4 and 0.2 µm pore size membranes, three times for each pore size. The same was done for CLs containing rhodamine, while DLs containing rhodamine were extruded two times through the 1.2 µm pore size membrane. SLNs containing rhodamine were extruded stepwise through 0.8 and 0.4 µm pore size membranes (three times each) and two times through 0.2 µm pore size membranes. All extruded CLs, DLs and SLNs were then kept in the fridge (+4 ºC) for a minimum of 3 h prior to characterisation and usage.

2.5. Size measurements

The particle size distributions of all CL, DL and SLN suspensions were determined by the dynamic light scattering [23] (NICOMP Submicron Particle Sizer Model 370; NICOMP Particle Sizing system, Santa Barbara, California, USA). The sample preparation was

performed in a laminar flow bench. Firstly, the test tubes were flushed once with KHb previously filtrated through 0.2 µm syringe filter (Bulk Acrodisc® 25 mm Syringe Filter, Pall Life Sciences, East Hills, New York, USA). The samples were diluted with the KHb to obtain a particle intensity between 250-350 kHz. The analyses were run in a vesicle mode for CLs and DLs, and solid particle mode for SLNs, respectively. Each measurement was done in triplicates (runtime of 10 min; 23-24 ℃). The size distributions of all nanocarriers, expressed as the mean diameter and polydispersity index (PI), were determined using the intensity-weighted distribution.

2.6. Zeta potential measurements

The zeta potential of liposomal and solid lipid nanoparticles suspensions was determined on Malvern Zetasizer Nano – ZS (Malvern, Oxford, UK) [24]. The instrument was calibrated with Malvern Zeta potential transfer standard (-42 ± 4.2 mV). A folded capillary cell (DTS1060) was used for the measurements. The cell was rinsed with ethanol and then with filtered water (0.2 µm syringe filter) prior to the sample. Each sample was diluted in a filtrated water (1:10 and 1:20 volume ratio for calcein- and rhodamine-containing nanocarriers, respectively) to achieve a suitable count rate. The diluted sample was injected into the folded capillary cell, assuring that no air bubbles formed during the injection. All measurements were performed at 25 ℃ with an equilibration time of 180 sec. Three measurement runs were performed for each sample, assuring an attenuator of 6-7.

2.7. Entrapment efficiency determination

The unentrapped calcein was separated from the extruded CLs, DLs and SLNs by dialysis. Typically, 5 mL of suspension were placed in a dialysis bag (Mw cut off 12,000-14,000 Da,

Medicell International Ltd, London, UK) and dialysed against 500 mL of KHb for 6 h at room temperature. The dialysis bag was immersed in fresh KHb (500 mL) and dialysis continued for additional 3 h. The volume of the receptor medium was chosen to assure the sink conditions. After the dialysis, CLs, DLs and SLNs were mixed with a Triton solution (5%, v/v) to dissolve the lipids before quantification of calcein by measuring fluorescence on a Polarstar fluorimeter (Fluostar; BMG Technologies, Offenburg, Germany) with excitation and emission wavelengths at 485 and 520 nm, respectively. Standard curves of calcein in KHb solution and calcein in Triton solution (5%, v/v) were used to determine the unentrapped and entrapped calcein, respectively. A concentration range between 0.12 and 1.37 µg/mL was used for both the standard curves (R^2 of minimum 0.9990). A blank consisting of KHb or Triton solution (5%, v/v) was subtracted from the fluorescence values.

Ultracentrifugation was performed to separate unentrapped rhodamine from CLs and SLNs, while gentle centrifugation was used for DLs. Extruded CLs and SLNs were centrifuged (Beckam model L8-70M ultracentrifuge with an SW 60 Ti rotor, Beckam Instruments, Palo Alto, California, USA) at 110,000 g for 1 h at 10 ℃. Extruded DLs were centrifuged (Biofuge stratos centrifuge with a swinging bucket rotor 4x 180 mL; Heraeus instruments GmbH, Hanau, Germany), at 3,000 g for 25 min at 10 ℃. The supernatants were separated from the pellets, which were resuspended in KHb. Lipids in both supernatants and pellets were dissolved in methanol and the rhodamine content was determined fluorometrically on a Polarstar fluorimeter (Fluostar; BMG Technologies, Offenburg, Germany) with excitation and emission wavelengths at 544 and 590 nm, respectively. To avoid evaporation of methanol during the fluorescence measurements, all samples were diluted in KHb to obtain a methanol concentration of 50% (v/v). The standard curve of rhodamine in methanol/KHb solution (1:1, v/v) was prepared using the concentrations ranging from 0.10 to 1.20 µg/mL (R^2 of minimum

0.9980). A blank consisting of methanol/KHb solution was subtracted from the fluorescence values.

The recovery of calcein and rhodamine was determined and found to be between 100.3 and 107.7%, respectively.

2.8. Phospholipid content

The phospholipid content in CLs, DLs and SLNs was determined to enable calculation of entrapment efficiency expressed as the marker/lipid ratio. A modification of Bartlett method was used [25]. In brief, all samples were diluted in distilled water (typically 1:200, v/v). An aliquot of diluted sample (1 mL) was mixed with sulfuric acid (5 M; 0.5 mL) and then incubated at 160 ºC for a minimum of 3 h. After the cooling, two drops of hydrogen peroxide 30% were added and the solutions incubated at 160 ºC for 1.5 h. After the cooling, ammonium molybdate (0.22%, w/v; 4.6 mL) and Fiske-Subbarow reducer (0.2 mL) were added, vortexed and incubated at 100 ºC for 7 min. The samples were then cooled down and analysed by ~~UV~~ UV-VIS spectrophotometry at 830 nm using a SpectraMax 190 Microplate Reader (Molecular Devices, California, USA)The standard curve was prepared using a phosphorus standard solution in a concentration range of 1-8 µg/mL (R^2 of minimum 0.9990).

2.9. Skin penetration experiments on IPHSF model

The skin penetration of calcein and rhodamine from CLs, DLs and SLNs was evaluated on the recently established IPHSF model [20]. The human skin flaps (the mean age of 49.3 years, range 26-72 years) were obtained from the abdominoplasty operations of female patients, after receiving their written consent prior to the surgery. The excess of skin and subcutaneous fatty tissue as residue after the surgery are normally disposed, therefore no ethical approval by

the Norwegian Ethical Committee was required. However, all experiments were performed in accordance with the Declaration of Helsinki Principles. Each formulation (CLs, DLs and SLNs containing either calcein or rhodamine) was tested in triplicates on three independent human skin flaps, obtained from different female donors. Human serum albumin (final concentration of 30 mg/mL) was included in the KHb to prepare the perfusate solution. The human skin flaps were cannulated and perfused with the perfusate within 90 min after their excision. The temperature of the perfusate entering the flap (inlet temperature) was maintained at approximately 32 ºC using a heating circulator set at 38 ºC. The use of an infrared (IR) camera (FLIR ONE, Thermal Imaging Camera for iOS; FLIR Systems) allowed the selection of the best perfused skin diffusion area (49 cm^2) having a skin temperature of *ca.* 32 ºC. The formulation (7 mL) was applied onto the selected perfused skin diffusion area using an adhesive patch as described by Ternullo and colleagues [20]. The experiments were carried out for 6 h and sampling was performed by collecting the perfusate every hour, assuring the sink conditions throughout the experiment. The physiological parameters, namely the perfusion inlet pressure, perfusion flow rate and inlet temperature, were recorded throughout the experiments [20]. To exclude oedema formation, the weight and thickness of each flap were measured before and at the end of the experiment. A weight and thickness variations of less than 10% was found acceptable. Blood cells were removed from the collected perfusate by the centrifugation (1914 *g*, 20 min), while plasma proteins were precipitated using trichloroacetic acid (58.82%, w/v) [20]. The obtained samples were then analysed fluorometrically, as described above, to quantify the penetrated markers through the full thickness IPHSF. Moreover, the amount of the markers retained onto the skin flap surface was determined fluorometrically.

2.9.1. Confocal laser scanning microscopy on IPHSF model

To localise the two markers in the IPHSF model after the skin penetration experiments, CLSM technique was employed [20] (Leica TCS SP5 microscope equipped with an Argon laser; Leica Microsystems CMS GmbH, Mannheim, Germany). Briefly, the imprint technique was used to prepare the samples. At the end of the skin penetration experiments, the treated perfused skin flap area was cut cross-sectionally and attached onto a microscope slide. Formalin (SPRAYFIX®, Histolab Products AB, Gothenburg, Sweden) was sprayed to fix the cells that remained on the slide. Laser lines of 488 and 568 nm were used to excite calcein and rhodamine, respectively. A spectral range of 500-550 nm and 570-610 nm were used to detect the calcein and rhodamine fluorescence, respectively.

2.10. In vitro skin penetration experiments

Franz diffusion cells (PermeGear, Bethlehem, USA) were used to perform *in vitro* skin penetration experiments following the method reported earlier [20]. Cells of 1.77 cm^2 diffusion area with a receptor volume of 12 mL were used. Cellophane membrane was pre-soaked in KHb for 30 min prior to the experiment. KHb constituted the receptor phase, which was maintained at 37 ℃ throughout the experiment to assure the physiological skin temperature of 32 ℃. CLs, DLs and SLNs containing either calcein or rhodamine were added to the donor chamber (sample volume of 600 µL). As controls, calcein in KHb and rhodamine in KHb/PG (0.5%, v/v) were used. The content of the two markers in the tested samples was determined fluorometrically prior to the penetration study and the concentration of markers in the donor chamber was equalised in all samples to assure the same concentration gradient. Sampling from the receptor chamber was done every hour for a period of 8 h. The withdrawn samples (500 µL) were replaced by an equal volume of fresh KHb to assure the sink conditions. All experiments were performed in triplicates. The markers penetrated through the

cellophane membrane and non-penetrated markers were quantified fluorometrically as described in section 2.7.

2.11. Ex vivo skin penetration experiments

Full thickness pig and human skin were used for *ex vivo* skin penetration studies [20]. Frozen pig ear skin slices were thawed, rinsed with water and cleared from the subcutaneous fat. Human skin was obtained from the resected skin during abdominoplasty of female patients, after their written consent was received. No ethical approval for the use of human skin was required by the Norwegian Ethical Committee, since the excess of skin panni is normally disposed after the surgery. The experiments were conducted in accordance with the Declaration of Helsinki Principles. The excised portion of human skin was rinsed with water and, after a removal of the subcutaneous fat, stored at -20 ºC and thawed 30 min before the start of the experiment. Each formulation and controls were tested in triplicates on human skin that was obtained from the same patient. Pig and human skin thicknesses were measured prior to the experiment and skin with thickness of approximately 1.50 mm was used. The skin was mounted into the same Franz diffusion cells used for the *in vitro* experiments; the SC side was facing the donor chamber. The tested formulations, receptor medium and sampling time were the same as in the *in vitro* skin penetration experiments (section 2.10). The markers Penetrated through the full thickness pig/human skin and non-penetrated markers were quantified as described in section 2.7.

2.12. Statistical analyses

The student's *t*-test (paired) was used to determine a statistical significance. A *p* value of less than 0.05 was considered statistically significant.

3. Results and discussion

Improved drug delivery to deeper skin layers could enable improved drug outcome in many topical therapies reducing the need for systemic treatment. However, the complex barrier of the skin, particularly the SC, which is the barrier responsible for rate-limiting step in skin drug penetration, should be addressed when designing/developing the dermal formulations [26]. Phospholipid-based nanocarriers have shown ability to enhance drug penetration through the SC and allow the sustained and controlled release of associated drugs [27-29]. The changes in the composition of phospholipid-based nanocarriers affect their interaction with the skin [14]. Therefore, a direct comparison of the skin penetration enhancement by the different phospholipid-based nanocarriers is helpful in the optimisation of efficient nanopharmaceuticals destined for localized skin therapy. The right choice of the nanocarrier would lead to the optimal therapeutic drug levels in the specific skin layers, and could be tailored for the specific skin disease.

3.1. Characteristics of the phospholipid-based nanosystems

Table 1 presents the characteristics of phospholipid-based nanosystems used in this study. The optimal size of nanocarriers for dermal drug delivery was proposed to be 200-300 nm [30]. The size of liposomes and solid lipid nanoparticles containing either calcein or rhodamine was between 200 and 300 nm, as targeted. The extrusion as a method for a vesicle/particle size reduction has shown to be a suitable method to obtain the desired vesicle/particle size and rather homogenous systems. The PI was found to be lower than 0.3 for all vesicles/particles (between 0.06 and 0.27) indicating relative homogeneity in size. Among the nanocarriers containing calcein, a significant difference ($p < 0.05$) in the size was observed for DLs, which

were smaller (201 nm) as compared to both CLs (265 nm) and SLNs (220 nm), respectively. Our finding is in accordance with literature [31-33]. The presence of SDCh in the phospholipid bilayers of DLs provides elasticity and flexibility to the liposomes, and reduces their surface tension. Rather homogenous size (PI < 0.3) was also obtained for rhodamine-containing nanocarriers. CLs and SLNs were of similar mean size (244 and 227 nm, respectively); a bimodal size distribution (Nicomp distribution) was observed for SLNs where a small percentage (6.5%) of smaller particles (24 nm) was found. DLs containing rhodamine were characterised by a bimodal size distribution (Table 1) as observed for SLNs. The main peak within the size distribution of DLs was higher (294 nm) compared to both CLs and SLNs; the of mean size of 294 nm exhibiting also the highest PI (0.27) was also the highest as compared to the other formulations. This size was obtained after only two cycles of extrusion through the polycarbonate membrane with 1.2 µm pore size membranes. Considering a potential pilot scale manufacturing, this could be considered an advantage regarding the manufacturing.

The surface charge of nanocarriers is also a factor that can play an important role in the skin penetration of associated drugs [34]. Our phospholipid-based nanosystems exhibited zeta potential in accordance with the nature of the material used for their preparation. CLs and SLNs containing either calcein or rhodamine had a zeta potential close to neutral, due to the main presence of neutral PC. DLs containing either calcein or rhodamine beard a strong negative surface charge, providing them with additional stability [21]. Although the skin has a net negative charge, negatively charged liposomes have shown to enhance skin drug penetration [34].

To assure improved skin deposition of nanocarrier-associated drugs, it is crucial to assure high drug load. In this study, we have used two different markers as model substances for a hydrophilic and a lipophilic drugs, respectively. The entrapment efficiencies for nanocarriers

containing calcein, expressed as a marker/lipid ratio, were not significantly different. Unexpectedly, DLs entrapped more calcein compared to CLs, although DLs were smaller. The presence of SDCh may increase the incorporation of this marker in DLs [35]. We expected a lower entrapment efficiency for SLNs, since they are known to possess low loading capacity for hydrophilic compounds [36]. However, Suter and collaborators [37] have recently demonstrated that SLNs might also incorporate high load of hydrophilic compounds, such as peptides, which is in agreement with our results. CLs containing rhodamine incorporated the highest amount of the marker compared to both DLs and SLNs (Table 1). The presence of SDCh in DLs decreased the entrapment efficiency, possibly due to a competition between rhodamine and SDCh both accommodated in the phospholipid bilayer of liposomes [31]. It is known that the lipids in SLN can re-crystallize into a highly ordered crystalline structure. This process can cause drug expulsion, reducing the entrapment efficiency [38]. Our results are in accordance with literature [39].

3.2 Penetration enhancing effect of the phospholipid-based nanocarriers in the IPHSF model

Optimisation of effective nanosystems for skin therapy requires validated skin penetration models. The recently established drug penetration (IPHSF) model was used for this purpose. The model offers the possibility of working with the presence of dermal circulation in the conditions similar to the *in vivo*, important parameter in the penetration studies [40]. The use of an IR camera allowed visualisation of the perfused skin flap area destined for the topical application of the tested formulations on the IPHSF model and served as a validation module of the model. IR images of the representative flaps taken during the experiments are shown in Fig. S1. The skin area, where the formulations were applied, was perfused throughout the whole penetration experiment. The physiological parameters were monitored during the experiment. The perfusion inlet pressure, flow and inlet temperature were adjusted to

maintain the perfusion of the human skin flaps (skin surface temperature of *ca*. 32 ºC).

Physiological parameters recorded during the skin penetration experiments in the IPHSF

model are shown in Fig. S2. Although the perfusion inlet pressures varied, the flap perfusion

was assured throughout the experiments and the variation of weight and thickness of flaps

was found to be less than 10% (data not included). The lower perfusion inlet pressures did not

affect the perfusion and the higher pressures did not cause oedema formation, which was

found acceptable. The temperature remained constant throughout the experiments.

No markers were found in the perfusate, indicating that our nanocarriers were not able to

deliver the two markers deeper into the dermis layer allowing them to become absorbed in the

systemic circulation. Therefore, all the investigated nanocarriers can be ~~be~~ used as drug

delivery systems for dermal, rather than transdermal drug therapy. This was expected

considering their size. However, the limited time (6 h) of the experiment should be

considered. Whether a longer time would permit some of the nanocarriers to penetrate deep

enough into the dermis to enable marker absorption remain to be addressed in *in vivo*

experiments. Our results are in accordance with Chen and colleagues [19], although their

studies were performed using human skin in the Franz diffusion cells. No permeation of the

tested markers through the full thickness human skin was observed in finite dose application

for all tested nanocarriers and only low percentages (0.001%) of the hydrophilic marker were

detected in the receptor fluid when the formulations were applied in infinite dose [19]. The

perfusion of the IPHSF could not be assured over a longer time (more than 6 hours), and we

assumed that the perfused skin should permit penetration <u>through the full thickness skin</u>

<u>barrier</u> at faster rate than the non-living skin. Assessment of the penetration potential of three

types of nanocarriers containing either calcein or rhodamine was also evaluated by the amount

of the marker retained on the top of the skin at the end of skin penetration experiments. Fig. 1

presents the percentages of the non-penetrated markers, indicating the markers retained on the

top of skin surface of the IPHSF. The rank order of the tested nanocarriers according to their capability to enhance the penetration of the two markers through the SC was CLs < DLs ≈ SLNs. DLs are expected to be more effective than CLs in drug transport across the skin [41]. Regarding SLNs, our results are in accordance with literature [27]. Clares and colleagues [27] did not find a significant difference in the permeation of retinyl palmitate from CLs and SLNs (4.36 and 3.64 µg, respectively) through human skin. However, SLNs were found to be more effective in enhancing the penetration into the upper SC, similar to our findings.

To assure that our assumption on the penetration within the SC was correct and visualise the differences between the investigated nanocarriers, a CLSM study was performed. The obtained confocal images (Fig. 2 and 3) supported our findings on the skin penetration profiles through the IPHSF model. Compared to the control (untreated human skin flap), fluorescence was detected in all skin samples, indicating a presence of marker. The delivery of the two markers into/through the skin layers was, however, dependent on the investigated nanocarriers. Calcein distribution through the IPHSF was found more uniform throughout the whole skin flaps treated with DLs (Fig. 2C) compared to CLs (Fig. 2B). This confirmed the better ability of DLs to enhance the skin penetration of the marker deeper through/into the skin layers. Earlier CLSM studies comparing skin-penetration depth of the hydrophilic marker fluorescein sodium from CLs and DLs showed stronger fluorescence and deeper penetration in the skin samples treated with DLs compared to CLs [42]. Although the authors performed the penetration study using the pig skin, the same results as obtained in our model were reported. Calcein from SLNs was found in the deeper skin layers (Fig. 2D) as compared to CLs-associated calcein. This indicates and confirms the ability of SLNs to enhance the penetration of calcein as a hydrophilic model substance through the SC. For rhodamine, the strongest fluorescence was found in SC and was not depend on the type of vesicles, in agreement with literature [19]. The weakest fluorescence was detected in the IPHSF treated

with the rhodamine-containing CLs (Fig. 3B), while the strongest was detected in the flaps treated with SLNs (Fig. 3D). DLs and SLNs assured higher penetration of rhodamine through/into the skin layers (Fig. 3C and 3D) compared to CLs. These results might be explained in part by the negatively charged surface of DLs; accumulation within the skin has shown to be more pronounced for negatively charged liposomes [14]. The enhanced penetration of lipophilic compounds from SLNs through the SC is also in agreement with literature [43,44].

The depth of the skin penetration of the two markers was clearly affected by the type of lipid-based nanocarriers the markers were associated with. The different composition of the nanocarriers plays a crucial role in determining their mechanism of action. CLs made of PC possess certain similarities with the SC lipids, which allow the fusion of the vesicles with the SC lipids, causing changes in the structure of the intercellular SC lipids. Therefore, CLs can act as penetration enhancers by loosening the lipid structure of the SC and lowering the permeability barrier of the skin. CLs can collapse onto the skin due to their fusion/mixing with the SC lipids, leading to the formation of an additional barrier and limiting the penetration of the incorporated drug to a higher extent [11].

When SDCh is incorporated in liposomes to form DLs, the skin penetration enhancing effect appears to be stronger. The presence of an edge activator in the lipid bilayer determines flexibility of the DLs and allows them to potentially squeeze into the corneocytes in the SC, thus delivering the drug deeper into the skin layers. Therefore, DLs appear to enhance drug penetration due to a synergistic effect between their deformability and their action as penetration enhancers. The deformability of DLs is also composition dependent. El Zaafarany and collaborators [28] have shown that the optimal deformability of DLs is reached when the ratio of phosphatidylcholine:edge activator is 85:15%, the same as used in our study. This further explains the capability of DLs in enhancing drug penetration into the skin compared to

CLs [28]. As discussed earlier, the surface charge of nanocarriers plays a role in the skin penetration of drugs. Our DLs were negatively charged and it has been shown that a negative vesicle surface charge increases drug skin penetration [14].

Regarding SLNs, two mechanisms of skin penetration enhancement are proposed; SLNs can adhere and fuse with the SC lipid [43] or they can form an occlusive film onto the skin surface preventing transepidermal water loss [29; 45]. The penetration enhancement of SLNs is dependent on the physicochemical properties of the encapsulated drug and the lipids. A stronger fluorescence observed for rhodamine as compared to calcein indicates that SLNs assured higher penetration of rhodamine through/into the skin layers (Fig. 3). This might be explained by the lipophilicity of the drugs, which affects the drug-particle interactions, the distribution of the drug within the SLNs and consequently the drug delivery by SLNs [46]. Küchler and collaborators performed electron spin resonance spectroscopy studies on SLNs using the spin probes with different lipophilicities. The authors showed that lipophilic probes were attached to the particles lipid surface, while hydrophilic probe was located in the layer of the surfactant. These distributions in the SLNs affected the skin penetration: the lipophilic probe penetrated faster and in a higher extent compared to the hydrophilic one [46], in agreement with our results. Similar studies have been performed by Saeidpour and collaborators [47], regarding the distribution of a lipophilic drug, dexamethasone, in SLNs. The authors found that the drug is located in the outer shell of the SLNs when immersed in aqueous solution but it can be easily released from the nanoparticles, which is in accordance to our results on rhodamine-containing SLNs (Fig. 3D).

When describing the skin penetration process of drugs, the interaction between the nanocarrier and the skin is not the only factor that has to be taken into account. The partitioning of the drug from the nanocarrier to the skin also plays a role in the skin penetration [19]. Comparing the penetration of calcein and rhodamine in the IPHSF model,

calcein was found to be more uniformly distributed throughout the skin layers (Fig. 2) compared to rhodamine (Fig.3), which was mainly accumulated in the SC. The percentage of non-penetrated calcein, a hydrophilic marker with a low log$P$ (-5.02), was higher compared to rhodamine that has lipophilic properties and higher log$P$ (1.95). The same behaviour was observed for all investigated nanosystems. The lipophilic rhodamine is mainly released from nanocarriers in the lipophilic environment provided by the SC [48], while the hydrophilic calcein is able to reach deeper into the hydrophilic dermal layer that is maintained perfused by KHb (hydrophilic medium) [20]. Therefore, dermal perfusion affected the skin penetration of the hydrophilic marker. Moreover, DLs and SLNs enhanced skin penetration of calcein to a higher extent compared to CLs, whereas the difference between DLs/SLNs and CLs was not observed for rhodamine (Fig. 1). This might be explained by the difference in lipophilicity of the two markers. For highly lipophilic compounds, such as rhodamine, the penetration enhancement by the nanocarriers is less evident because they possess the intrinsic capacity to move with relative ease through the SC. In the case of hydrophilic substances such as calcein, the nanocarriers have the opportunity to act as penetration enhancer due to the low partition coefficient of hydrophilic compounds [19].

3.3 In vitro and ex vivo skin penetration

All nanocarriers exhibited a sustained permeation of calcein through the cellophane membrane compared to the control (calcein in KHb solution) (Fig. 4A). Among the investigated nanocarriers, the highest calcein permeation was observed from CLs. DLs are known to increase the penetration of incorporated drugs due to their elasticity [31]. We did not observe this typical mechanism of action for DLs in our *in vitro* studies. A possible explanation might be due to their net negative surface charge (-32 mV), which is similar to the charge of cellophane membranes [49]. Since both surfaces have negative zeta potentials, the

energy barrier might prevent DLs deposition on the cellophane membrane, interfering with calcein penetration through the barrier. SLNs permitted the lowest calcein penetration of calcein through the barrier, in agreement with reported studies on SLNs incorporating hydrophilic compounds [38,50].

Rhodamine permeation profiles from all nanocarriers through the cellophane membrane are presented in Fig. 4B. Both CLs and SLNs were able to sustain the permeation of rhodamine, as expected for lipophilic compounds [27,29]. However, SLNs sustained rhodamine release to a higher extent compared to CLs. The presence of a solid lipid matrix in SLNs, in contrast with the fluid core of liposomes, reduces the mobility of the incorporated drugs. This might assure a more controlled release of the drug from the SLNs compare to CLs [51]. The highly ordered crystalline structure of the SLNs strongly accommodates the drug and slows the drug release [38]. DLs containing rhodamine exhibited the highest marker penetration through the barrier. Although a charge repulsion between the DLs and cellophane membrane might be relevant for the calcein penetration (Fig. 4A), for rhodamine the observed higher a higher release, compared to the other nanocarriers, might be contributed to the lipophilicity of the marker. Rhodamine is accommodated in the bilayer of DLs, while calcein is incorporated in the inner aqueous core. Therefore, rhodamine is more likely to be released from DLs even with a possible charge repulsion of DLs with the cellophane membrane.

Skin permeation of calcein from nanocarriers through the full thickness pig skin is shown in Fig. 4C. The amount of penetrated calcein through the full thickness pig skin from all nanocarriers was lower compared to *in vitro* studies (cellophane membrane). A sustained release of calcein from all nanocarriers was obtained compared to the control. DLs assured higher calcein penetration through the full thickness pig skin compared to CLs and SLNs, as expected [42]. These results also confirmed that the lower calcein permeation from DLs observed in *in vitro* studies (Fig. 4A) might be due to charge repulsion between DLs and

cellophane membrane. Skin penetration of rhodamine from nanocarriers through the full thickness pig skin (Fig. 4D) showed similar trend as in *in vitro* studies as well as in literature [52]. However, no significant difference was observed among the nanocarriers and the penetration of rhodamine through the full thickness pig skin was lower from all nanocarriers compared to *in vitro* studies. Both markers, regardless of the nanocarrier types, were not found to permeate the full thickness human skin in the Franz diffusion cells system (data not shown). Therefore, the skin penetration through the full thickness human skin in the Franz diffusion system appears to closely resemble the penetration observed in our IPHSF model. This highlights the importance of using the human skin in the skin penetration studies. The amount of non-penetrated markers (retained on the top of the different skin membrane models) was quantified at the end of *in vitro* and *ex vivo* skin penetration experiments to compare the penetration determined on the IPHSF model with the established skin models. Fig. 5 represents a summary of the two markers penetration through the *in vitro* and *ex vivo* full thickness skin models. As discussed earlier, all nanocarriers exhibited lower penetration of calcein compared to the control both through the cellophane membrane and full thickness pig skin; while no calcein was detected in the receptor medium when full thickness human skin was tested in Franz diffusion cells system. Moreover, all nanocarriers were able to retain higher amount of calcein on the top of the skin in all tested skin models as compared to the control (Fig. 5A). Retention of calcein on the top of the human skin in the Franz diffusion cells system and IPHSF model were comparable, except for SLNs. SLNs mediated a lower retention of associated calcein on the IPHSF model compared to *ex vivo* human skin. This might be explained by the fact that the perfusion of human skin flap is performed with an aqueous medium (KHb), which can influence skin penetration of hydrophilic compounds [20].

Retention of rhodamine on the top of all skin models is shown in Fig. 5B. The non-penetrated amount of rhodamine was found to be lower compared to calcein, in agreement with data obtained from the IPHSF model. Our results indicate that rhodamine remained accumulated within the SC, due to its lipophilic nature. Among the investigated nanocarriers, CLs and SLNs assured higher retention of rhodamine on all the skin models, while DLs were able to enhance rhodamine penetration through the full thickness skin barriers. DLs containing rhodamine were earlier tested in the pig skin by Carrer and co-authors [53]. The authors found that negatively charged DLs, as our DLs, were able to increase a marker penetration through the pig skin to a greater extent. CLs and SLNs did create a drug reservoir in the skin [53]. Jensen and collaborators [29] tested the penetration properties of SLNs containing corticosteroids, lipophilic drugs, in the pig skin and compared SLNs with an ointment. The penetration of the drug through the intact skin was reduced when the drug was formulated in SLNs and a higher amount of drug remained in the upper layers of the skin [29], in agreement with our findings. DLs exhibited the lowest retention of rhodamine on the human skin in Franz diffusion cells compared to the other nanocarriers. This suggests that DLs improved the penetration of the marker through the human SC. Skin penetration studies and two-photon microscopy analysis from Simonsson and collaborators [54] support our findings. Although they tested rhodamine-containing ethosomes, they found an increased penetration of rhodamine from ethosomes compared to the hydroethanolic solution. Moreover, as we observed in the CLSM studies on the IPHSF model, they also observed a strong fluorescence from rhodamine in the SC when incorporated in ethosomes. Penetration of rhodamine from all nanocarriers through the IPHSF model was found to be more similar to the *ex vivo* human skin than through cellophane membrane and pig skin; the same trend as observed for calcein. Although the penetration profile observed for all nanocarriers incorporating either calcein or rhodamine through all the full thickness skin barrier models was the same, the retention of the

two markers on the top of cellophane membrane and pig skin differed significantly ($p < 0.03$) from the human skin and IPHSF model. The artificial membranes have already shown their limited ability to reflect the complex interactions between the human skin and the applied formulations, often resulting in non-comparable findings [55]. Although pig ear skin is more able to represent *in vivo* human skin than artificial membranes [56], recent studies have shown that frozen/thawed pig skin is more permeable than freshly excised skin. It has been postulated that the high ceramide and low cholesterol levels in pig skin might cause an easy disruption of the SC due to ice crystalline formation. This leads to impaired SC barrier and thus higher permeability of drugs [57]. Moreover, especially for pig skin, the total recovery of both markers was reported to be lower than the stated ideal value ($100 \pm 15\%$) [58]. Although we only quantified the markers penetrated through the full thickness skin barriers and non-penetrated markers and did not extract any markers retained in the barriers, it might be hypothesised that the impaired SC barrier of frozen/thawed pig skin favours the retention of the markers, especially the lipophilic rhodamine, within the skin. Therefore, the low recovery might be explained by the non-considered amount of markers retained in the skin. Moreover, the markers penetrated through the full thickness skin barriers and non-penetrated amounts of both markers were calculated from the content of the two markers in the formulations determined fluorometrically prior to the penetration study. Therefore, another possible explanation for the low recovery might be an underestimation of the marker content, determined prior to the experiment, from the theoretical amount.

The results indicate that it is crucial to test the nanocarriers on the reliable skin models able to mimic *in vivo* studies as close as possible and that the direct comparison of various nanocarriers can serve as an important step in development of the optimal dermal formulation targeting a specific dermal condition. It is necessary to note that the described nanocarriers will require a suitable vehicle to assure their retention on the skin.

4. Conclusions

This study confirmed the different skin penetration potential of three phospholipid-based nanocarriers using the IPHSF model, a model closely resembling the human studies. The differences in their lipid nanocarriers composition and surface charge determined their mechanism of action and a different skin penetration depth of the two markers. DLs and SLNs exhibited higher penetration of the two markers compared to CLs through the isolated perfused human skin flap model. Moreover, DLs and SLNs delivered both markers deeper into the skin layers compared to CLs. This comparative study could serve in the optimisation of phospholipid-based nanosystems for localized skin therapy and assist in the right selection of the nanocarrier for targeted drug delivery into the specific skin layers, depending on the targeted skin condition/disease.

References

1. R.J. Hay, N.E. Johns, H.C. Williams, I.W. Bolliger, R.P. Dellavalle, D.J. Margolis, R. Marks, L. Naldi, M.A. Weinstock, S.K. Wulf, C. Michaud, C.J.L. Murray, M. Naghavi, The global burden of skin disease in 2010: an analysis of the prevalence and impact of skin conditions, J. Invest. Dermatol. 134 (2014) 1527-1534.

2. M. Gupta, U. Agrawal, S.P. Vyas, Nanocarrier-based topical drug delivery for the treatment of skin diseases, Expert Opin. Drug Deliv. 9 (2012) 783-804.

3. R. Goyal, L.K. Macri, H.M. Kaplan, J. Kohn, Nanoparticles and nanofibers for topical drug delivery, J. Control. Release. 240 (2016) 77-92.

4. S.G. Ingebrigtsen, A. Didriksen, M. Johannessen, N. Škalko-Basnet and A. Mari Holsæter, Old drug, new wrapping – A possible comeback for chloramphenicol? Int. J. Pharm. 526 (2017) 538-546.

5. R. Banerjee, Overcoming the stratum corneum barrier: a nano approach, Drug Deliv. Transl. Res. 3 (2013) 205-208.

6. H.C. Korting, M. Schäfer-Korting, Carriers in the topical treatment of skin disease, in: M. Schäfer-Korting (Ed.), Drug Delivery, Handbook of Experimental Pharmacology 197, Springer-Verlag Berlin Heidelberg, Berlin, 2010, pp. 435-468.

7. L.A. DeLoiuse, Applications of nanotechnology in dermatology, J. Invest. Dermatol. 132 (2012) 964-975.

8. R. Saraceno, A. Chiricozzi, M. Gabellini, S. Chimenti, Emerging applications of nanomedicine in dermatology, Skin Res. Technol. 19 (2013) 13-19.

9. A. Patzelt, W.C. Mak, S. Jung, F. Knorr, M.C. Meinke, H. Richter, E. Rühl, K.Y. Cheung, N.B.N.N. Tran, J. Lademann, Do nanoparticles have a future in dermal drug delivery? J. Control. Release. 246 (2017) 174-182.

10. B. Geusens, T. Strobbe, S. Bracke, P. Dynoodt, N. Sanders, M. Van Gele, J. Lambert, Lipid-mediated gene delivery to the skin, Eur. J. Pharm. Sci. 43 (2011) 199-211.

11. S. Fireman, O. Toledano, K. Neinmann, N. Loboda, N. Dayan, A look at emerging delivery systems for topical drug products, Dermatol. Ther. 24 (2011) 477-488.

12. J. de Leeuw, H.C. de Vijlder, P. Bjerring, H.A.M. Neumann, Liposomes in dermatology today, J. Eur. Acad. Dermatol. Venereol. 23 (2009) 505-516.

13. G. Cevc, G. Blume, Lipid vesicles penetrate into intact skin owing to the transdermal osmotic gradients and hydration force, Biochim. Biophys. Acta. 1104 (1992) 226-232.

14. M.L. González-Rodríguez, A.M. Rabasco, Charged liposomes as carrier to enhance the permeation through the skin, Expert Opin. Drug Deliv. 8 (2011) 857-871.

15. J. Kristl, K. Teskač, P.A. Grabnar, Current view on nanosized solid lipid carriers for drug delivery to the skin, J. Biomed. Nanotechnol. 6 (2010) 529-542.

16. D. Papakostas, F. Rancan, W. Sterry, U. Blume-Peytavi, A. Vogt, Nanoparticles in dermatology, Arch. Dermatol. Res. 303 (2011) 533-550.

17. A. Lauterbach, C.C. Müller-Goymann, Applications and limitations of lipid nanoparticles in dermal and transdermal drug delivery via the follicular route, Eur. J. Pharm. Biopharm. 97 (2015) 152-163.

18. S. Doktorovová, A.B. Kovačević, M.L. Garcia, E.B. Souto, Preclinical safety of solid lipid nanoparticles and nanostructured lipid carriers: Current evidence from *in vitro* and *in vivo* evaluation, Eur. J. Pharm. Biopharm. 108 (2016) 235-252.

19. M. Chen, X. Liu, A. Fahr, Skin penetration and deposition of carboxyfluorescein and temoporfin from different lipid vesicular systems: In vitro study with finite and infinite dosage application, Int. J. Pharm. 408 (2011) 223-234.

20. S. Ternullo, L. de Weerd, G.E. Flaten, A.M. Holsæter, N. Škalko-Basnet, The isolated perfused human skin flap model: A missing link in skin penetration studies? Eur. J. Pharm. Sci. 96 (2017) 334-341.

21. Z. Palac, J. Hurler, N. Škalko-Basnet, J. Filipović-Grčić, Ž. Vanić, Elastic liposomes-in-vehicle formulations destined for skin therapy: the synergy between type of liposomes and vehicle, Drug Dev. Ind. Pharm. 41 (2015) 1247-1253.

22. M.A. Schubert, C.C. Müller-Goymann, Solvent injection as a new approach for manufacturing lipid nanoparticles – evaluation of the method and process parameters, Eur. J. Pharm. Biopharm. 55 (2003) 125-131.

23. M.W. Jøraholmen, Ž. Vanić, I. Tho, N. Škalko-Basnet, Chitosan-coated liposomes for topical vaginal therapy: Assuring localized drug effect, Int. J. Pharm. 472 (2014) 94-101.

24. S.G. Ingebrigtsen, N. Škalko-Basnet, C. de Albuquerque Cavalcanti Jacobsen, A.M. Holsæter, Successful co-encapsulation of benzoyl peroxide and chloramphenicol in liposomes by a novel manufacturing method - dual asymmetric centrifugation, Eur. J. Pharm. Sci. 97 (2017) 192-199.

25. G.R. Bartlett, Phosphorus assay in column chromatography, J. Biol. Chem. 234 (1959) 466-468.

26. G.K. Menon, G.W. Cleary, M.E. Lane, The structure and function of the stratum corneum, Int. J. Pharm. 435 (2012) 3-9.

27. B. Clares, A.C. Calpena, A. Parra, G. Abrego, H. Alvarado, J.F. Fangueiro, E.B. Souto, Nanoemulsions (NEs), liposomes (LPs) and solid lipid nanoparticles (SLNs) for retinyl palmitate: effect on skin permeation, Int. J. Pharm. 473 (2014) 591-598.

28. G.M. El Zaafarany, G.A.S. Awad, S.M. Holayel, N.D. Mortada, Role of edge activators and surface charge in developing ultradeformable vesicles with enhanced skin delivery, Int. J. Pharm. 397 (2010) 164-172.

29. L.B. Jensen, K. Petersson, H.M. Nielsen, *In vitro* penetration properties of solid lipid nanoparticles in intact and barrier-impaired skin, Eur. J. Pharm. Biopharm. 79 (2011) 68-75.

30. J. du Plessis, C. Ramachandran, N. Weiner, D.G. Müller, The influence of particle size of liposomes on the deposition of drug into the skin, Int. J. Pharm. 103 (1994) 277-282.

31. A. Gillet, F. Lecomte, P. Hubert, E. Ducat, B. Evrard, G. Piel, Skin penetration behaviour of liposomes as a function of their composition, Eur. J. Pharm. Biopharm. 79 (2011) 43-53.

32. Z. Palac, A. Engesland, G.E. Flaten, N. Škalko-Basnet, J. Filipović-Grčić, Ž. Vanić, Liposomes for (trans)dermal drug delivery: the skin-PVPA as a novel *in vitro stratum corneum* model in formulation development, J. Liposome Res. 24 (2014) 313-322.

33. Ž. Vanić, A. Hafner, M. Bego, N. Škalko-Basnet, Characterization of various deformable liposomes with metronidazole, Drug Dev. Ind. Pharm. 39 (2013) 481-488.

34. A. Gillet, P. Compère, F. Lecomte, P. Hubert, E. Ducat, B. Evrard, G. Piel, Liposome surface charge influence on skin penetration behaviour, Int. J. Pharm. 411 (2011) 223-231.

35. A.P.C.O. Bahia, E.G. Azevedo, L.A.M. Ferreira, F. Frézard, New insights into the mode of action of ultradeformable vesicles using calcein as hydrophilic fluorescent marker, Eur. J. Pharm. Sci. 39 (2010) 90-96.

36. J. Pardeike, A. Hommoss, R.H. Müller, Lipid nanoparticles (SLN, NLC) in cosmetic and pharmaceutical dermal products, Int. J. Pharm. 366 (2009) 170-184.

37. F. Suter, D. Schmid, F. Wandrey, F. Zülli, Heptapeptide-loaded solid lipid nanoparticles for cosmetic anti-aging applications, Eur. J. Pharm. Biopharm. 108 (2016) 304-309.

38. G. Zoubari, S. Staufenbiel, P. Volz, U. Alexiev, R. Bodmeier, Effect of drug solubility and lipid carrier on drug release from lipid nanoparticles for dermal delivery, Eur. J. Pharm. Biopharm. 110 (2017) 39-46.

39. K. Ferderber, S. Hook, T. Rades, Phosphatidyl choline-based colloidal systems for dermal and transdermal drug delivery, J. Liposome Res. 19 (2009) 267-277.

40. U.F. Schaefer, S. Hansen, M. Schneider, J. Luengo Contreras, C.M. Lehr, Models for skin absorption and skin toxicity testing, in: K. Kim, K.J. Ehrhardt (Eds.), Drug Absorption Studies: In Situ, In Vitro and in Silico Models, Springer, New York, 2008, pp. 3-33.

41. T. Uchino, F. Lefeber, G. Gooris, J. Bouwstra, Characterization and skin permeation of ketoprofen-loaded vesicular systems, Eur. J. Pharm. Biopharm. 86 (2014) 156-166.

42. T. Subongkot, S. Duangjit, T. Rojanarata, P. Opanasopit, T. Ngawhirunpat, Ultradeformable liposomes with terpenes for delivery of hydrophilic compound, J. Liposome Res. 22 (2012) 254-262.

43. L. Vidlářová, J. Hanuš, M. Veselý, P. Ulbrich, F. Štěpánek, J. Zbytovská, Effect of lipid nanoparticle formulations on skin delivery of a lipophilic substance, Eur. J. Pharm. Biopharm. 108 (2016) 289-296.

44. J. Chen, N. Wei, M. Lopez-Garcia, D. Ambrose, J. Lee, C. Annelin, T. Peterson, Development and evaluation of resveratrol, Vitamin E, and epigallocatechin gallate loaded lipid nanoparticles for skin care applications, Eur. J. Pharm. Biopharm. 117 (2017) 286-291.

45. L.M. Andrade, C. de Fátima Reis, L. Maione-Silva, J.L.V. Anjos, A. Alonso, R. Caixeta Serpa, R. Neves Marreto, E. Martins Lima, S. Fleury Taveira, Impact of lipid dynamic behavior on physical stability, *in vitro* release and skin permeation of genistein-loaded lipid nanoparticles, Eur. J. Pharm. Biopharm. 88 (2014) 40-47.

46. S. Küchler, W. Herrmann, G. Panek-Minkin, T. Blaschke, C. Zoschke, K.D. Kramer, R. Bittl, M. Schäfer-Korting, SLN for topical application in skin diseases-Characterization of drug-carrier and carrier-target interactions, Int. J. Pharm. 390 (2010) 225-233.

47. S. Saeidpour, S.B. Lohan, A. Solik, V, Paul, R. Bodmeier, G. Zoubari, M. Unbehauen, R. Haag, R. Bittl, M.C. Meinke, C. Teutloff, Drug distribution in nanosctructured lipid particles, Eur. J. Pharm. Biopharm. 110 (2017) 19-23.

48. G. Bastiat, C.O. Pritz, C. Roider, F. Fouchet, E. Lignières, A. Jesacher, R. Glueckert, M. Ritsch-Marte, A. Schrott-Fischer, P. Saulnier, J-P. Benoit, A new tool to ensure the fluorescent dye labeling stability of nanocarriers: A real challenge for fluorescence imaging, J. Control. Release. 170 (2013) 334-342.

49. M.Y. Boluk, T.G.M. van de Ven, Effects of polyelectrolytes on flow-induced deposition of titanium dioxide particles onto a cellophane surface, Colloids Surf. 46 (1990) 157-176.

50. L.G. Souza, E.J. Silva, A.L.L. Martins, M.F. Mota, R.C. Braga, E.M. Lima, M.C. Valadares, S.F. Taveira, R.N. Marreto, Development of topotecan loaded lipid nanoparticles for chemical stabilization and prolonged release, Eur. J. Pharm. Biopharm. 79 (2011) 189-196.

51. H.S. Jeon, J.E. Seo, M.S. Kim, M.H. Kang, D.H. Oh, S.O. Jeon, S.H. Jeong, Y.W. Choi, S. Lee, A retinyl palmitate-loaded solid lipid nanoparticle system: Effect of surface modification with dicetyl phosphate on skin permeation *in vitro* and anti-wrinkle effect *in vivo*, Int. J. Pharm. 452 (2013) 311-320.

52. C.M.S. Cereda, M. Franz-Montan, C.M.G. da Silva, B.R. Casadei, C. Crepaldi Domingues, G. Radomille Tofoli, D. Ribeiro de Araujo, E. de Paula, Transdermal

delivery of butamben using elastic and conventional liposomes, J. Liposome Res. 23 (2013) 228-234.

53. D.C. Carrer, C. Vermehren, L.A. Bagatolli, Pig skin structure and transdermal delivery of liposomes: A two photon microscopy study, J. Control. Release. 132 (2008) 12-20.

54. C. Simonsson, J.T. Madsen, A. Graneli, K.E. Andersen, A-T. Karlberg, C.A. Jonsson, M.B. Ericson, A study of the enhanced sensitizing capacity of a contact allergen in lipid vesicle formulations, Toxicol. Appl. Pharmacol. 252 (2011) 221-227.

55. C. Herkenne, A. Naik, Y.N. Kalia, J. Hadgraft, R.H. Guy, Ibuprofen transport into and through skin from topical formulations: *in vitro-in vivo* comparison, J. Invest. Dermatol. 127 (2007) 135-142.

56. P.W. Wertz, Current understanding of skin biology pertinent to skin penetration: skin biochemistry, Skin Pharmacol. Physiol. 26 (2013) 217-226.

57. A.C. Sintov, Cumulative evidence of the low reliability of frozen/thawed pig skin as a model for *in vitro* percutaneous permeation testing, Eur. J. Pharm. Sci. 102 (2017) 261-263.

58. T. Haque, K.M. Rahman, D.E. Thurston, J. Hadgraft, M.E. Lane, Topical delivery of anthramycin I. Influence of neat solvents, Eur. J. Pharm. Sci. 104 (2017) 188-195.

Figures and figure legends:

Fig. 1. Skin penetration of calcein and rhodamine from phospholipid-based nanocarriers (CL, DL, SLN) through the IPHSF model.

The penetrated amount (marker in perfusate) was below detectable level in all skin penetration experiments (6 h). The non-penetrated markers were quantified after 6 h experiments. Results are presented as mean ± SD (n = 3).

Fig. 2. Representative CLSM images of calcein-in-nanocarriers in IPHSF after 6 h of skin penetration experiments.

The IPHSF was cross-sectionally cut, starting from the skin surface (upper side) to the subcutaneous fatty tissue (lower side). (A) Control, untreated IPHSF. (B), (C) and (D) IPHSF treated with calcein-containing CLs, DLs and SLNs, respectively.

Fig. 3. Representative CLSM images of rhodamine-in-nanocarriers in IPHSF after 6 h of skin penetration experiments.

The IPHSF was cross-sectionally cut, starting from the skin surface (upper side) to the subcutaneous fatty tissue (lower side). (A) Control, untreated IPHSF. (B), (C) and (D) IPHSF treated with rhodamine-containing CLs, DLs and SLNs, respectively.

Fig. 4. Penetration profiles of calcein (left column) and rhodamine (right column) from CLs, DLs and SLNs through the cellophane membrane (A, B) and full thickness pig skin (C, D) using the Franz diffusion cells.

As control, calcein in KHb and rhodamine in KHb/PG (0.5%, v/v) were used. The concentration of markers was equalised in all tested formulations to assure the same

concentration gradient. The skin penetration experiments were carried out for a period of 8 h and results are presented as the mean ± SD (n = 3). $^*p < 0.05$.

Fig. 5. *In vitro* **and skin penetration studies (8 h) of calcein (A) and rhodamine (B) from CLs, DLs and SLNs through the cellophane membrane, full thickness pig skin and human skin using the Franz diffusion cells (n = 3).**

As control, calcein in KHb and rhodamine in KHb/PG (0.5%, v/v) were used. Calcein and rhodamine concentrations were equalised in all tested formulations to assure the same concentration gradient.

Tables and table legends:

Table 1. Characteristics of phospholipid-based nanocarriers containing calcein or rhodamine (n = 3 ± SD).

[a] The diameter is expressed as the peaks in size distributions (nm) and weight intensity of each peak (%), which is indicated in parentheses

[b] Polydispersity index

[c] $p < 0.05$

[d] Bimodal size distribution

Supplementary material and Supp. Figures legends:

Fig. S1. IR images of the representative human skin flaps taken during 6 h of skin penetration experiments.

(A) IR images recorded before application of the formulations. (B), (C) and (D) IR images recorded at time 0, 3 and 6 h after the application of the formulations, respectively. A perfused skin area (skin temperature at *ca*. 32 ºC) was assured throughout the experiment.

Fig. S2. Physiological parameters recorded throughout the skin penetration experiments (6 h).

Values are presented as the mean ± SD (n = 3).

Fig. 1. Skin penetration of calcein and rhodamine from phospholipid-based nanocarriers (CL, DL, SLN) through the IPHSF model. The penetrated amount (marker in perfusate) was below detectable level in all skin penetration experiments (6 h). The non-penetrated markers were quantified after 6 h experiments. Results are presented as mean ± SD (n = 3).

Fig. 2. Representative CLSM images of calcein-in-nanocarriers in IPHSF after 6 h of skin penetration experiments. The IPHSF was cross-sectionally cut, starting from the skin surface (upper side) to the subcutaneous fatty tissue (lower side). (A) Control, untreated IPHSF. (B), (C) and (D) IPHSF treated with calcein-containing CLs, DLs and SLNs, respectively.
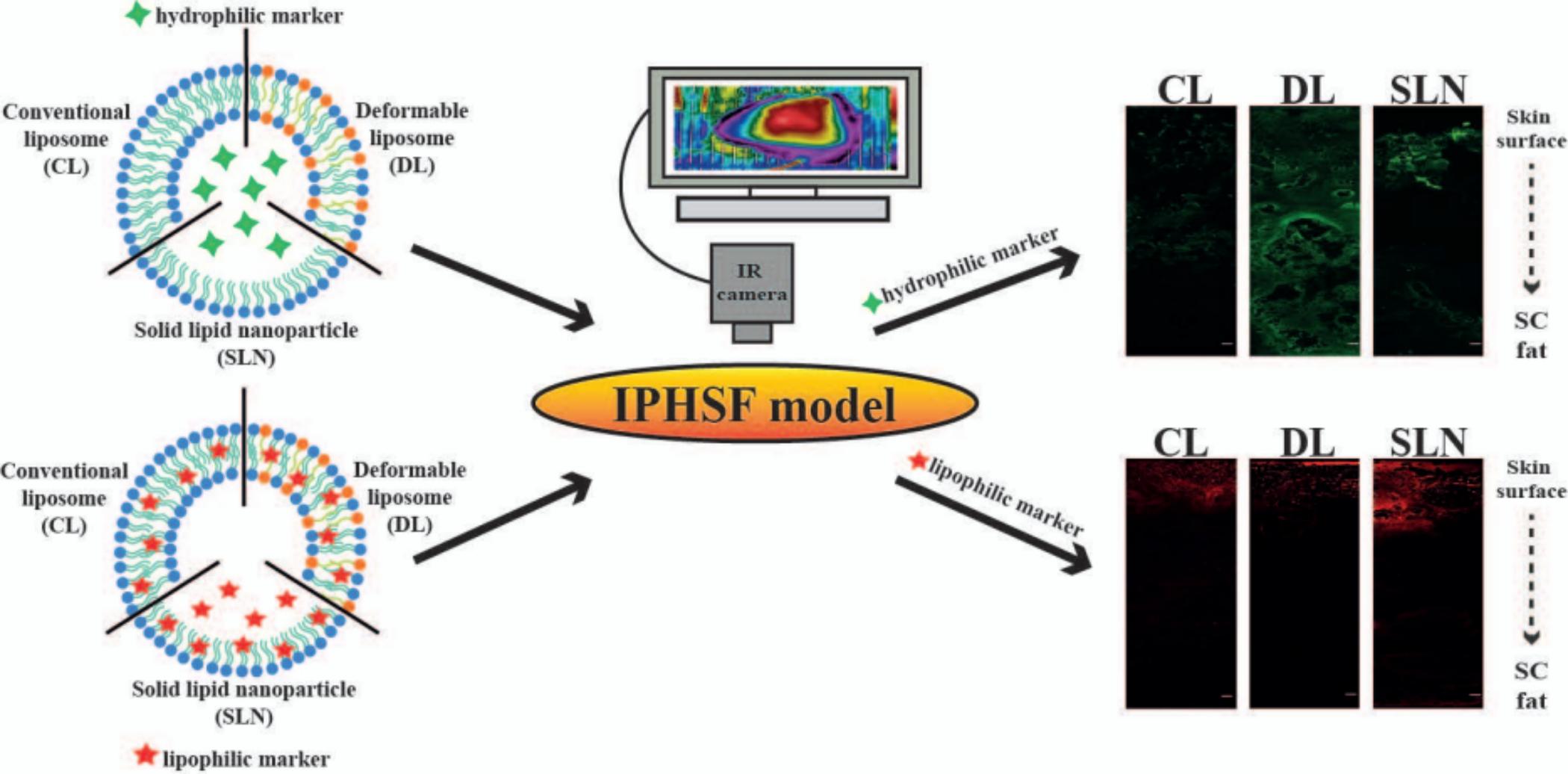
Fig. 3. Representative CLSM images of rhodamine-in-nanocarriers in IPHSF after 6 h of skin penetration experiments. The IPHSF was cross-sectionally cut, starting from the skin surface (upper side) to the subcutaneous fatty tissue (lower side). (A) Control, untreated IPHSF. (B), (C) and (D) IPHSF treated with rhodamine-containing CLs, DLs and SLNs, respectively.
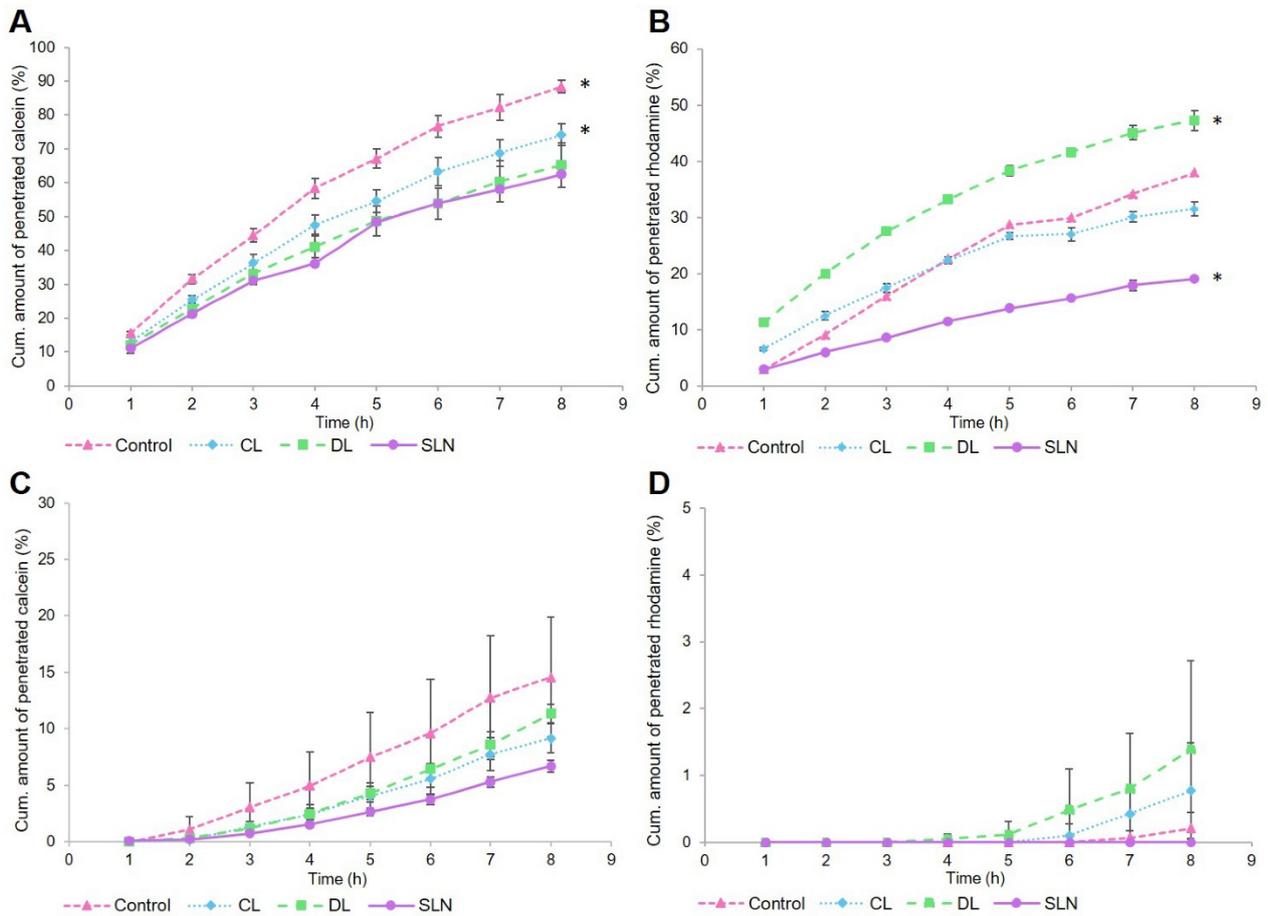
Fig. S1. IR images of the representative human skin flaps taken during 6 h of skin penetration experiments. (A) IR images recorded before application of the formulations. (B), (C) and (D) IR images recorded at time 0, 3 and 6 h after the application of the formulations, respectively. A perfused skin area (skin temperature at *ca*. 32 ℃) was assured throughout the experiment.
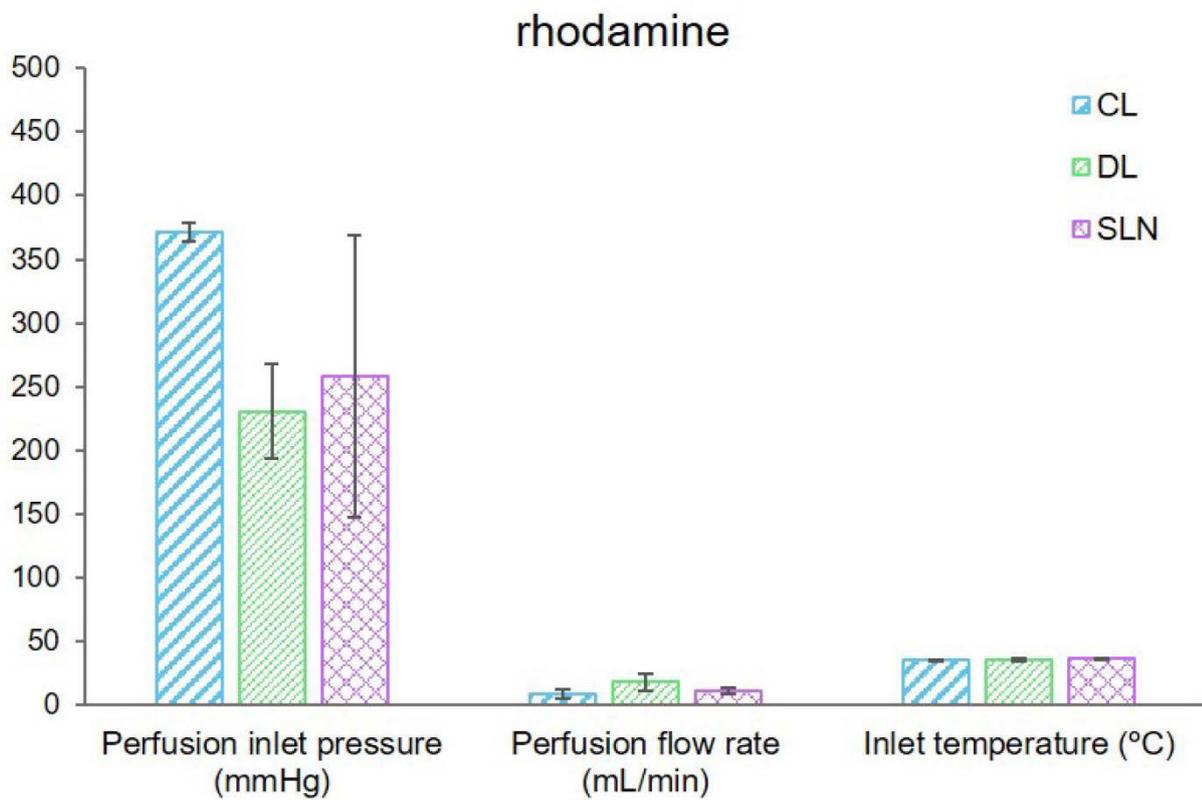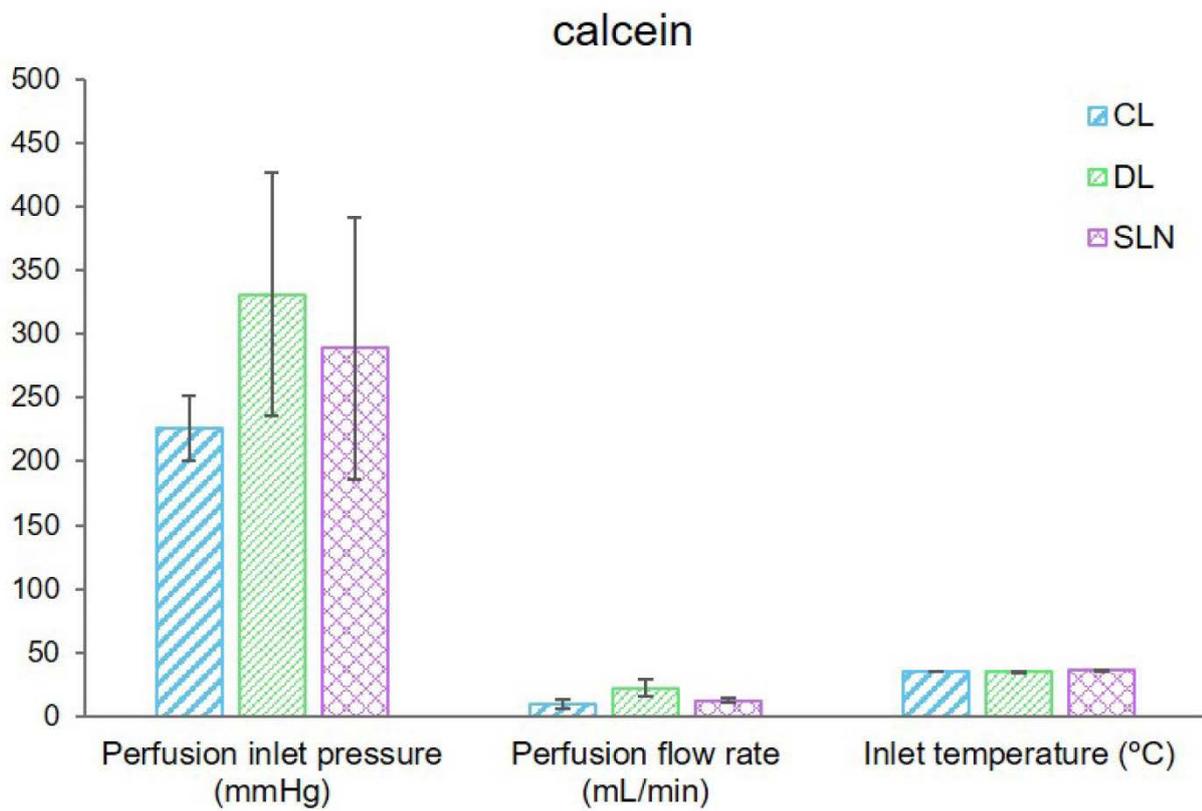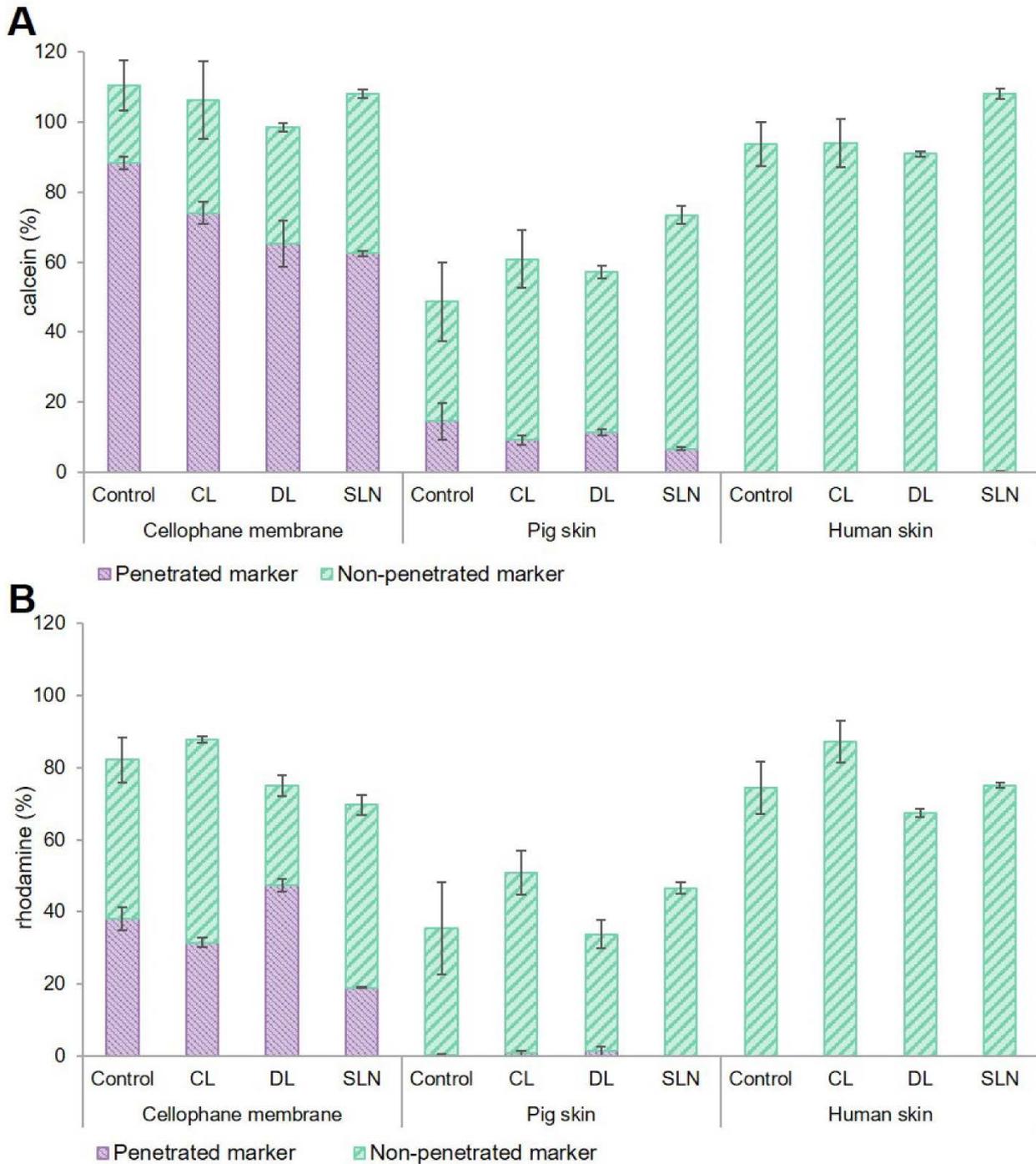
Fig. S2. Physiological parameters recorded throughout the skin penetration experiments (6 h).

Values are presented as the mean ± SD (n = 3).

Fig. 4. Penetration profiles of calcein (left column) and rhodamine (right column) from CLs, DLs and SLNs through the cellophane membrane (A, B) and <u>full thickness </u>pig skin (C, D) using the Franz diffusion cells. As control, calcein in KHb and rhodamine in KHb/PG (0.5%, v/v) were used. The concentration of markers was equalised in all tested formulations to assure the same concentration gradient. The skin penetration experiments were carried out for a period of 8 h and results are presented as the mean $\pm$ SD (n = 3). $^{*}p < 0.05$.

Fig. 5. *In vitro* and skin penetration studies (8 h) of calcein (A) and rhodamine (B) from CLs, DLs and SLNs through the cellophane membrane, full thickness pig skin and human skin using the Franz diffusion cells (n = 3). As control, calcein in KHb and rhodamine in KHb/PG (0.5%, v/v) were used. Calcein and rhodamine concentrations were equalised in all tested formulations to assure the same concentration gradient.